Zheng *et al.*
Progress in Earth and Planetary Science (2022) 9:12
https://doi.org/10.1186/s40645-022-00470-x

Progress in Earth and Planetary Science

RESEARCH ARTICLE Open Access

From desert to monsoon: irreversible climatic transition at ~ 36 Ma in southeastern Tibetan Plateau

Hongbo Zheng[1,2*], Qing Yang[1], Shuo Cao[3], Peter D. Clift[1,4], Mengying He[5], Akihiro Kano[6], Aki Sakuma[6], Huan Xu[1], Ryuji Tada[1,7] and Fred Jourdan[8]

Abstract

Although there is increasing evidence for wet, monsoonal conditions in Southeast Asia during the late Eocene, it has not been clear when this environment became established. Cenozoic sedimentary sequences constrained by radiometrically dated igneous rocks from the Jianchuan Basin in the southeast flank of Tibetan Plateau now provide a section whose facies and climatic proxies determine this evolution. Semi-arid conditions had dominated the region since Paleocene controlled by the northern sub-tropical high pressure system, culminating in mid Eocene when desert dunes developed. From 36 Ma, the basin began to accumulate swamp sediments with coals, together with synchronous braided river deposits and diversified pollen assemblages, indicating significant increase in precipitation. This remarkable transition from dry to wet conditions precedes the Eocene/Oligocene boundary at 34 Ma, thus excluding general global cooling as the prime driver. We propose that uplift of Tibetan Plateau might have reached a threshold elevation by that time, operating through thermal and dynamic forcing, causing the inception or significant intensification of monsoonal rains to penetrate into this downwind locality.

Keywords: Desert, Late Eocene, Onset of Asian monsoon, Tibetan Plateau

1 Introduction

The Asian monsoon is the global type example of how the solid Earth and atmosphere interact with one another in order to drive significant climate change (Webster et al. 1998; Wang 2010) (Fig. 1). Although it is clear that there are several processes that affect the intensity of the Asian summer monsoon (e.g., solar insolation, ocean temperatures and glacial cycles), there is little doubt that the present strong intensity is at least partly related to the uplift of the Himalaya in the case of the South Asian monsoon (Boos and Kuang 2010), as well as the elevation and broadening of the Tibetan Plateau in East Asia (Molnar et al. 2010; Tada et al. 2016). It has been proposed that at least parts of southern Tibet may have been elevated to significant altitude (i.e., similar to today) before the collision between India and Eurasia (Najman et al. 2010), generally dated at around 50–60 Ma (Najman et al. 2010; DeCelles et al. 2014; Wu et al. 2014; Hu et al. 2016). Nonetheless, there is little doubt that compressional deformation, lithospheric delamination and under thrusting of Indian crust under the active continental margin of Eurasia must have driven significant uplift of rock and likely the Earth's surface following the onset of collision (Wang et al. 2008; Xu et al. 2013). This raises the possibility that the monsoon might have intensified shortly after the start of collision, despite the fact most climatic reconstructions date its initiation to being much later (Gupta et al. 2015; Sun and Wang 2005; Clift et al.

*Correspondence: zhenghb@ynu.edu.cn
[1] Yunnan Key Laboratory of Earth System Science, Yunnan University, Kunming 650500, China
Full list of author information is available at the end of the article

2008). Indeed, climatic modeling supports such a view, showing that some degree of monsoon circulation would be sustainable within the framework of continental distribution and paleo-latitudes at the time (Huber and Goldner 2012; Carmichael et al. 2016), if not before the collision.

The prediction of an early onset to the monsoon is, however, largely in conflict with much existing paleoclimate and oceanographic data, although it should be recognized that there are relatively few records from the Eocene or Oligocene. Early reconstructions of the monsoon that were derived from scientific ocean drilling records in the Indian Ocean pointed toward initial intensification only after around 8 Ma (Kroon et al. 1991; Prell et al. 1992). The 8 Ma age was consistent with other constraints, such as the stable isotope data linked to the types of vegetation in the NW Himalayan foreland basin (Quade et al. 1989), as well as with dust records in the North Pacific (Rea 1994). This view was subsequently superseded by reconstructions that favored strengthening around the start of the Miocene, around 24 Ma (Sun and Wang 2005; Clift et al. 2008; Guo et al. 2002), and reduction in intensity in the late Miocene. If collision started at 50–60 Ma, then why would intensification be delayed so long?

In contrast to the multitude of Neogene records, documentation of environmental conditions during the Paleogene is substantially less well developed, a situation that makes it hard to test for an early onset monsoon. This partly reflects the scarcity of suitable sections to study. A major unconformity in the Himalayan foreland basin has removed much of the upper Eocene and Oligocene record in that region (Najman 2006). While suitable records are likely preserved in the marine basins around Asia these sediments for the most part are deeply buried under younger deposits, so that they are often out of reach of most drilling technology and have only been seismically imaged except in the shallowest parts (Curray et al. 2002; Clift et al. 2001). Nonetheless, information has begun to point to monsoonal climatic conditions much earlier than previously recognized. In southern China, leaf morphologies have been used to argue for a weak monsoon similar in the style to the Indonesian-Australian system in that area by the Eocene (Spicer et al. 2016). In the NE Tibetan Plateau, the Xining Basin (Fig. 1) was found to contain a sequence of Eocene lake deposits including evaporites overlain by Oligocene fluvial sedimentary rocks. This sequence was interpreted to indicate drying across the Eocene Oligocene boundary (~33.6 Ma) (Dupont-Nivet et al. 2007). Although evaporites are generally associated with desiccating, hot environments they do require the presence of a water source in order to supply material to evaporate. This discovery implied that there was more precipitation in the Eocene than in the subsequent Oligocene. These authors suggested that this transition from wetter conditions into more arid ones was driven by the sharp cooling and global climate across this boundary (Zachos et al. 2001).

Further information concerning Eocene climate was derived from the recognition in the Xining Basin of Upper Eocene eolian sedimentary rocks (Mahalagou Formation) dated between 40 and 33 Ma (Fig. 1) (Licht et al. 2014). Because the source of these sediments was toward the west of the basin, it was inferred that these materials were transported by westerly winter monsoon-related circulation. This implies that an atmospheric pattern with similarities to the present day had been established at this time. Whether this really indicates the establishment of summer monsoon rains is another question, because the winter and summer monsoons do not necessarily develop in parallel with one another, despite sometimes showing some degree of linkage (Talbot 1990). Windblown silt is, however, not an indicator of rainfall intensity. Further support for a Late Eocene monsoon was supplied in the form of oxygen isotope data from Myanmar (Licht et al. 2014) (Fig. 1). These data were measured from growth rings in gastropods and showed a strong seasonality, a typical feature of the monsoon. The isotopic composition of calcite in shells is derived from the water from which is precipitated, that in turn reflects rainwater compositions. As a result, these values are often interpreted as a proxy for rainfall intensity (Talbot 1990). Rainwater becomes more negative in $\delta^{18}O$ with heavier rainfall, although the source of the water is also a significant influence, albeit harder to constrain (Gat 1980; Rozanski et al.1993). The shell-derived $\delta^{18}O$ data argued for there being both wet and dry seasons in the Late Eocene (Licht et al. 2014). However, some concerns remain because Myanmar is now, and was then, in a relatively coastal situation where precipitation might occur regardless of there being a monsoon system or not.

Stronger evidence for an Eocene monsoon has come from the Jianchuan Basin of Yunnan in SW China, positioned on the SE flank of the Tibetan Plateau (Fig. 1). This lies in a much more continental setting and requires the rain front to penetrate far into the continent in order to provide significant precipitation. Although for a long time, the sediments in this basin were believed to date from the Paleocene up to the Pliocene recent re-dating of the section (Gourbet et al. 2017), supported by new constraints presented here, demonstrated that some of the youngest sedimentary rocks in the basin are Upper Eocene. These data constrain the deposition of the Shuanghe Formation (coal series) to being between 36

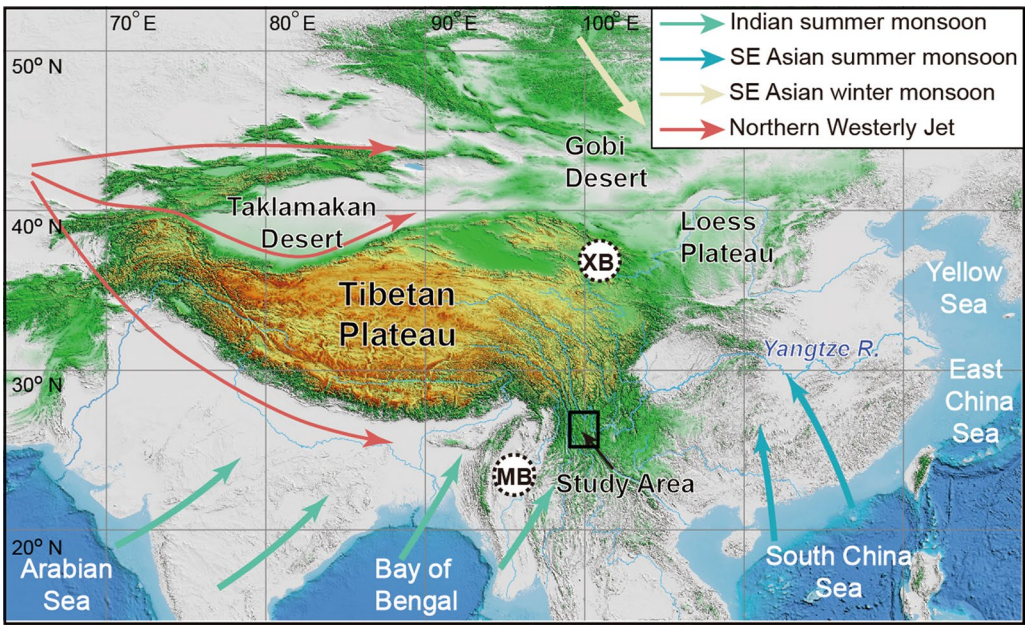

Fig. 1 Location map showing the DEM of Tibetan Plateau and surrounding regions. Also showing are the general climatic configuration (Westerly Jet, South Asian monsoon and Southeast Asian monsoon). Xining Basin and central Myanmar Basin are marked by XB and MB, respectively. Note that the present-day northern Westerly Jet is deflected into northern and southern branches owing to the orographic effects of Tibetan Plateau

and around 35 Ma, based on radiometric ages of igneous intrusions and volcanic rocks, with ages of around 35 Ma being found in the overlying Jianchuan Formation. Sorrel et al. (2017) interpreted the Shuanghe Formation, a sequence of fluvial sandstones, siltstones, shales and interbedded coals as having been deposited in a swamp forest environment that was established before 35.5 Ma. They considered the Jiuziyan Formation, a limestone, to underlie the Shuanghe Formation and to represent wet conditions, but slightly more temperate and arid than the overlying swampy sequences. They further proposed that this transition was indicative of a monsoon climate established before 35.5 Ma.

In this study, we present new high-resolution radiometric data that support and extend the age assignment of Gourbet et al. (2017), but we re-interpret the stratigraphy of the Jianchuan Basin to argue that the wet conditions of the Shuanghe Formation (and the Jinsichang Formation) were preceded by an prolonged arid period and that there was a well-defined, rapid transition from arid to humid at ~ 36 Ma, predating by around 2 m.y. the climate transition of the Xining Basin at the Eocene–Oligocene boundary. We argue that the climatic wettening at 36 Ma represents the first major onset of summer monsoon rains and that this was not linked to global climate but rather to uplift of the Tibetan Plateau.

2 Geological setting and lithostratigraphy

The Jianchuan basin is one of several in the SE flank of the Tibetan Plateau, whose origin is tied to the Cenozoic strike-slip faulting associated with the process of "extrusion" of rigid tectonic blocks away from the India-Eurasia collision zone (Figs. 1 and 2A) (Morley 2002; Tapponnier et al. 2001). Earlier mapping had suggested that this was a long-lived basin spanning Paleocene to Pliocene (Yunnan Bureau of Geology and Mineral Resources 1990; Mountney 2012), but with disputed chronostratigraphy owing to the lack of absolute age anchors. Recent radiometric dating of volcanic rocks, tuff and volcano-sedimentary rocks interbedded in the sequences has enabled the reconstruction of a stratigraphy with much higher age precision (Yang et al. 2014; Gourbet et al. 2017; Zheng et al. 2020), which is now further refined by new ages provided in this study. The following describes the lithologic formations of Cenozoic rocks from Jianchuan Basin, in the context of new chronology.

Yunlong Formation: Cenozoic sedimentary sequences start with Yunlong Formation which is composed of dark red, mudstone and siltstone (Fig. 2B, C). Regional stratigraphic correlation suggests that the Yunlong Formation (termed Mengyanjing Formation by Gourbet et al. (2017)), although sparsely exposed in Jianchuan Basin,

is widespread across the SE margin of Tibetan Plateau and is of Paleocene age. Facies analysis indicates that the Yunlong Formation was deposited in a fluvial-lacustrine setting under a relatively arid regime, although one still requiring some precipitation.

Baoxiangsi Formation: The Yunlong Formation is overlain by the Baoxiangsi Formation (Fig. 2B), which makes up the largest single part of the basin fill, with a thickness up to ~ 600 m.

The lower part of Baoxiangsi Formation is composed predominantly of conglomerate and coarse sandstone (Fig. 2B, D–F). Bedding is often thick (> 1 m), and erosive contacts place poorly sorted, matrix-supported conglomerate over coarse to medium grained sandstones, which are often massive in character, but locally show trough cross-bedding testifying to high energy current-driven sedimentation. The provenance of the conglomerates is spatially heterogeneous across the basin, suggestive of quite localized sources and short transport distances that preclude large-scale mixing. Facies analysis indicates that much of the lower Baoxiangsi Formation was deposited in a proximal alluvial fan and/or associated braided river systems (Zheng et al. 2020).

The upper part of Baoxiangsi Formation, with an average thickness of ~ 200 m, consists mainly of dark red, thick-bedded sandstone with large-scale, high-angle trough and planar cross-bedding (Fig. 2G). Superposed large-scale, high-angle trough and planar cross-bedded sandstones are interpreted as eolian dune facies (Brookfield and Silvestro 2010) (Fig. 3A, B). In these deposits, the upper cross-bedding truncates the underlying one to form a superimposition surface (S). Although the cross-bedded sandstones are just the remaining bedforms from the original primary dunes (Mountney 2012), the thickness of individual beds and bedding sets still exceeds 6 m and tens of meters, respectively. Wavelengths range from tens to hundreds of meters in length. The cross-bedding can be further divided into grainfall and grainflow strata (gf), as well as wind ripple strata (wr), which interfinger with one another and could reflect seasonal winds changes (Loope et al. 2001). As the reactivation surfaces (R) result from periodic migration, they are common in every eolian cross-bedding set. The interdune facies association is composed of both arid and moist interdune units. Moist interdune deposits are only observed in marginal parts of the basin, consisting of wavy laminated sandstones, adhesion-rippled sandstones and small-scale contorted bedded sandstones. Arid interdune units are widespread throughout the basin and are commonly interbedded with the dune units. Arid interdune sediments are dominated by low-angle translatent wind-ripple strata, separated from the dune sandstones by interdune migration surfaces (I), but they share the same source of sand as the dune sediments, so that there is no difference in composition between the two units.

Further investigation of thin sections, grain size distribution and surface morphology of quartz grains under scanning electron microscope (SEM) provides more evidence to support an eolian origin (Fig. 3C). The sandstones are grain-supported quartz arenites, lithic or feldspathic quartz sandstones, consisting dominantly of quartz and minor feldspar, as well as lithic fragments and rare mica and clay minerals. The particles are medium to fine grained, sub-rounded to rounded, well-sorted. In addition, the grains are covered by a distinct thin coating of iron oxides that formed under relatively dry conditions. The results of the grain size analysis show a clear unimodal distribution in percentage histograms and typical single stage distributions in log-probability grain-size distribution curves, indicating the presence of a dominant saltation population with minor amounts of traction and suspension populations. SEM images of the quartz grains show that most of the grains are in the rounded and well-rounded classes, although subrounded and subangular grains can also be seen. Dish- and crescent-shaped impact scars, elongated depressions and adhering particles are commonly present. These surface characteristics all point toward sedimentation in an eolian dune environment (Garzanti 2018).

Jinsichang Formation: Across most of the basin, the Baoxiangsi Formation is overlain by the Jinsichang Formation (~ 300 m thick and amalgamated with the Baoxiangsi by Gourbet et al. (2017) (Fig. 2B, H). This formation is characterized by horizontally bedded, cross-bedded, medium-grained sandstone sets, with beds up to 2 m thick, interbedded with minor mudstone. These beds can be found amalgamated into stacks of beds tens of meters thick, usually palely yellowish colored and contrasting with the redder, muddier rocks of the Baoxiangsi Formation. The Jinsichang Formation is interpreted to have been deposited in a major fluvial system, likely braided in character, given the lack of overbank facies (Miall 1977; Zheng et al. 2020).

Jiuziyan Formation: The Jiuziyan Formation consists of a multi-story carbonate succession interbedded with massive, matrix-supported conglomerates and argillaceous calcisiltites (Fig. 2I). The Jiuziyan Formation is restricted to a limited area in the central part of Jianchuan Basin, with a thickness of up to several tens of meters. The Jiuziyan Formation has previously been interpreted as being a marine deposit (Li et al. 1988). However, recent studies suggested that it was deposited in a palustrine-lacustrine environment (Sorrel et al. 2017; Sakuma et al. 2021). The Jiuziyan Formation is characterized by micritic and microspar to sparry limestones, with interbedded marls and conglomerates. Fossil reeds,

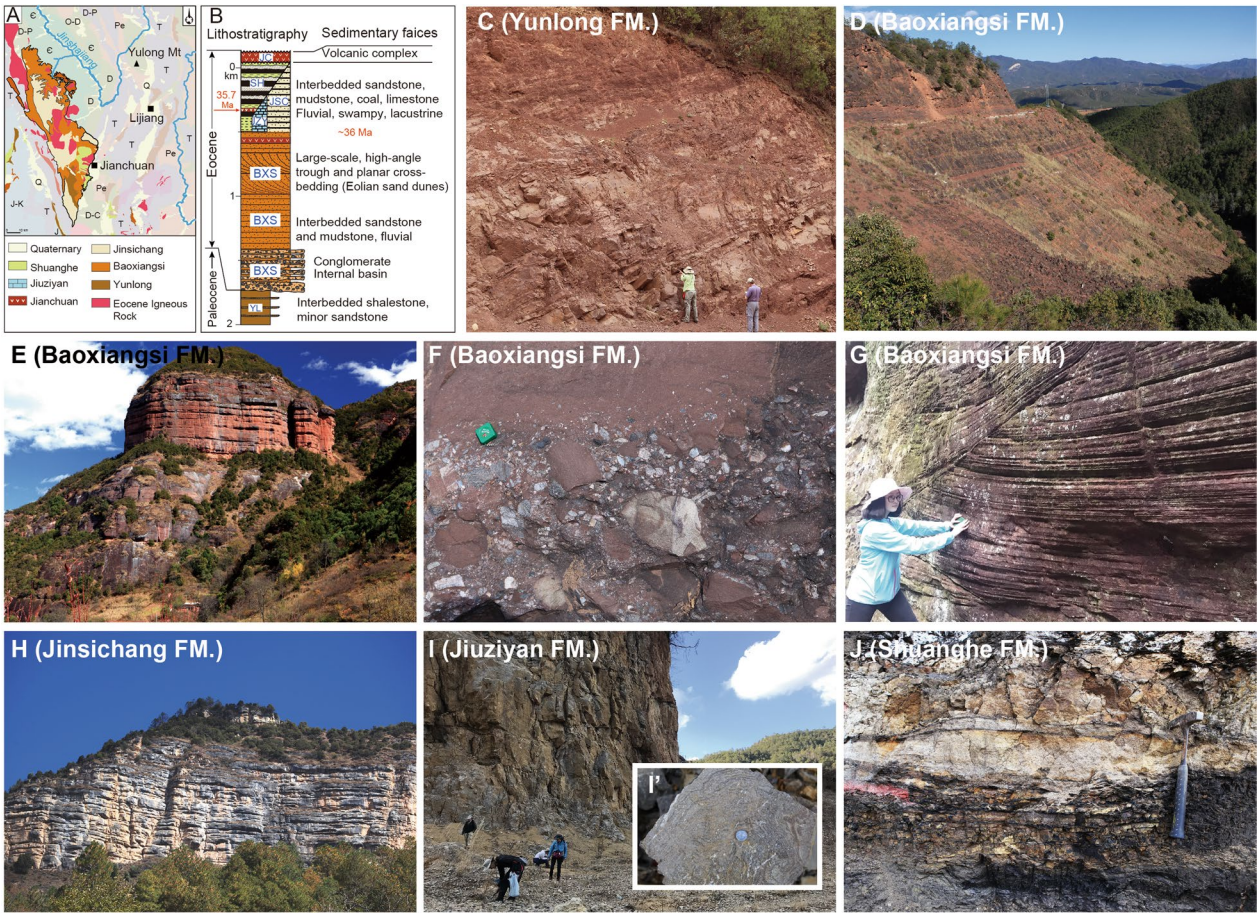

Fig. 2 **A** Cenozoic geology map of Jianchuan Basin; **B** lithostratigraphy of Cenozoic successions of Jianchuan Basin, with emphasis on sedimentary facies; **C** Yunlong Formation showing red weathered siltstones interbedded with minor sandstones and conglomerates; **D** Red, thin to medium bedded sandstones interbedded with conglomerates of the Baoxiangsi Formation; **E** Massive think-bedded conglomerates of Baoxiangsi Formation; **F** Poorly sorted fanglomerate and sandstones of the Baoxiangsi Formation; **G** Upper Baoxiansi Formation, showing dark red, thick-bedded sandstones with large-scale, high-angle trough and planar cross-bedding; **H** Stacked, thick-bedded typical pale colored sandstones of the Jinsichang Formation; **I** Massive thick-bedded limestone of the Jiuziyan Formation, and stromatolites within the limestone (**I'**); **J**, Shuanghe Formation, showing coals with interbedded fine sandstones, siltstones, shales, and volcano-sedimentary rocks

oncolite and stromatolites are locally abundant. The Jiuziyan Formation was assigned a Paleocene to Middle Eocene age by Li et al. (1988), based on the fossil assemblages. Our new stratigraphic investigation indicates that it is Late Eocene in age.

Jiuziyan carbonates crystalized in an enclosed water body (Sakuma et al. 2021), or a travertine setting similar to Baisuitai in northern Yunnan province described by Liu et al. (2010). The calcium of these deposits was likely fed by springs, as indicated by isotope values. Part of the Jiuziyan Formation shows laminated structures from which oxygen-carbon isotopes were analyzed (Fig. 4). Generally, high $\delta^{13}C$ (+2 to +7‰) and low $\delta^{18}O$ (< −10‰) indicate an endogenic origin of CO_2 and high temperature or low $\delta^{18}O$ of water (see Supplementary Information for analytical details). The samples show laminated structures consisting of dark and light layers of a few mm to 1 cm thick. The dark layers are porous, peloidal, and generally high in $\delta^{13}C$, while the light layers are densely calcified and low in $\delta^{13}C$ (Fig. 4). The dark and light layers are interpreted to represent dry/cold and wet/humid seasons, respectively. This seasonality is a feature of a monsoon climate.

Shuanghe Formation: The Shuanghe Formation is about 200 m thick, consisting of poorly consolidated sandstones and marlstones regularly interbedded with coal deposits (that thicken upwards) and occasional lava flows, tuffs and volcano-sedimentary levels (Fig. 2J). The distribution of the Shuanghe Formation is restricted to the central part of Jianchuan Basin, where the Jinsichang

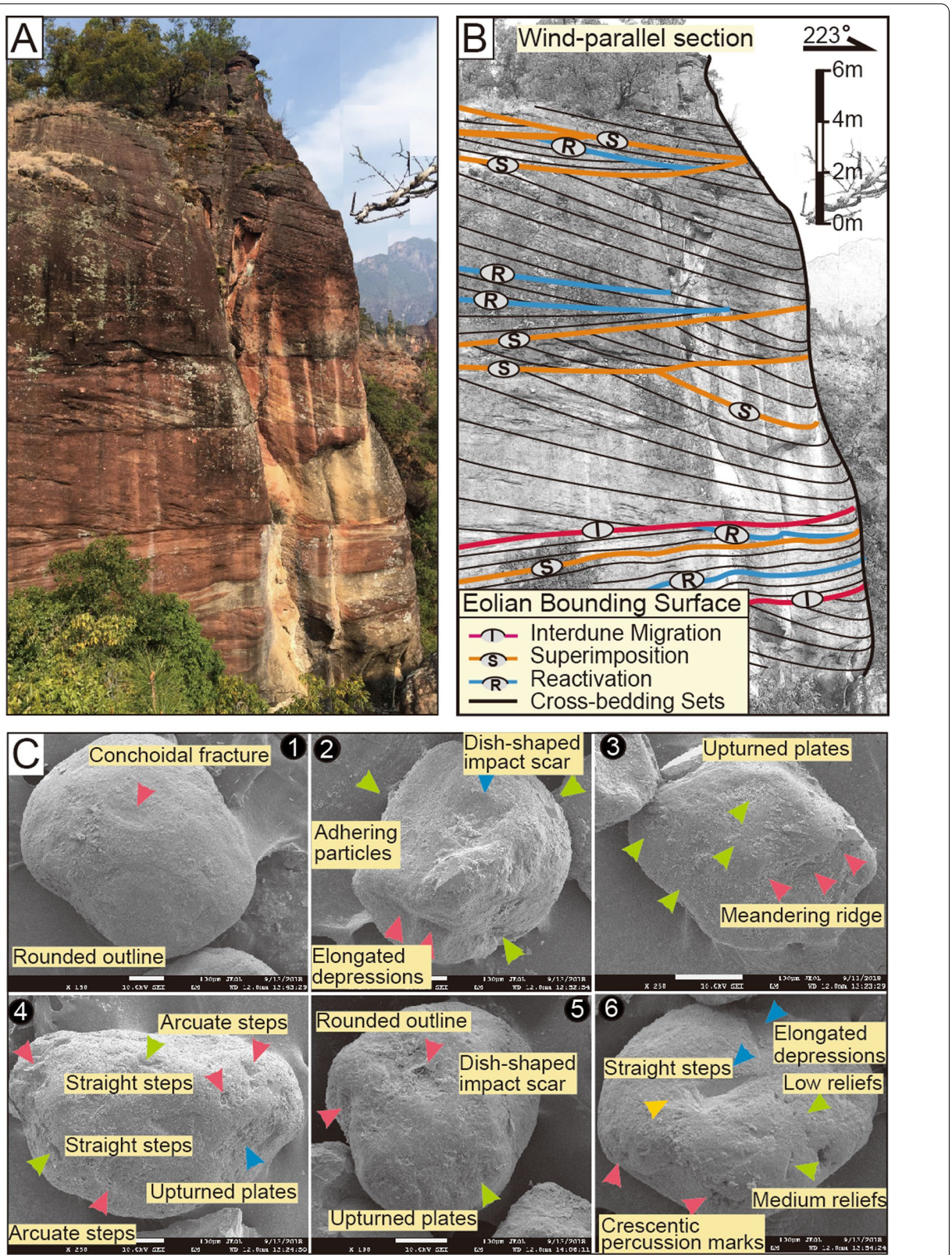

Fig. 3 Photographs and micrographs evidences of eolian dune deposits from Baoxiangsi Formation. **A** Photograph of eolian dune deposits from Baoxiangsi Formation; **B** Line drawing architecture and eolian bounding surfaces of **A**. Wind-parallel section shows large-scale eolian cross-beddings. **C** Micrographs of quartz grains of eolian dune deposits from Baoxiangsi Formation

Formation is absent. The Shuanghe Formation in observed to overly the Baoxiangsi Formation conformably in some places. But in many cases, the contact of Shuanghe Formation with the underlying unit is hard to observe due to poor exposure.

In previous studies, the Baoxiangsi (including the Jinsichang Formation) was interpreted to be over lain by a carbonate interval, the Jiuziyan Formation, and in turn by the Shuanghe Formation (Gourbet et al. 2017; Yunnan Bureau of Geology and Mineral Resources 1990). However, in our reassessment of the basin fill we combine the Jinsichang, Jiuziyan and Shuanghe Formations into a single unit, with the different formations representing contrasting lateral facies changes across the basin (Fig. 2B). We note that in the SE Jianchuan basin the Shuanghe Formation overlies the Baoxiangsi Formation conformably without any intervening Jinsichang or Jiuziyan Formations, as seen further north (Fig. 2A).

We concur with Sorrel et al. (2017) that deposition of the Shuanghe Formation represents sedimentation under relatively humid conditions, as shown by the presence of coals interbedded with medium-bedded fluvial sandstones and shales, likely of a meandering river facies, based on the presence of channelized sands and tabular muddy overbank facies (Smith 1987) (Fig. 2B). Sandstones frequently show the imprint of wood and leaf debris showing the presence of a vibrant flora. Pollen studies show that *Pinus* is still present, together with *Quercus*, *Poaceae* (grasses) and occasional *Cyperus*, spanning temperate to tropical settings (refer to Palynological Study). Polypodiaceae ferns are also common in this formation, and critically these are distinctive of wet conditions, often rain forests (Mathews et al. 2013). The Shuanghe Formation is cut by intrusive rocks (mostly lamprophyres), which form numerous sills in the coal-rich levels, as well as occasional lava flows, tuff and volcano-sedimentary levels (Fig. 2J). We note that the Shuanghe Formation is restricted to the central and eastern parts of Jianchuan Basin, where the Jinsichang Formation is absent (Fig. 2A). We therefore propose that the two formations were deposited at the same time, but as lateral facies equivalents. This sequence was then covered by the Jianchuan Formation (0–300 m thick), which mostly consists of volcaniclastic deposits related to the magmatism that intrudes the section.

Jianchuan Formation: Jianchuan Formation overlies unconformably on Shuanghe and Jinsichang Formations (Fig. 2B). It has previously been assigned a Pliocene age (Yunnan Bureau of Geology and Mineral Resources 1990). Jianchuan Formation consists mainly of pyroclastic rocks, volcanic tuff and volcano-sedimentary rocks.

3 Samples, methods and results

3.1 $^{40}Ar/^{39}Ar$ dating and Chronostratigraphy

We prepared sanidine and/or biotite single-crystal aliquots from a pyroclastic flow (sample #140902-04) from the Shuanghe Formation and a biotite (#141021-01) and muscovite (#140903-05) crystal populations from two lamprophyre intrusions and a sanidine population (#140902-05) from a trachyte intrusions, all of them cross-cutting the Shuanghe Formation. The various were carefully hand-picked under a binocular microscope in order to select the freshest and inclusion-free crystals. The selected crystals were thoroughly rinsed with distilled water in an ultrasonic cleaner. Samples were loaded into large wells of one 1.9 cm diameter and 0.3 cm depth aluminum discs. These wells were bracketed by small wells that included Fish Canyon sanidine (FCs) used as a neutron fluence monitor for which an age of 28.294 ± 0.036 Ma (1σ) was adopted (Renne et al., 2011). The discs were Cd-shielded (to minimize undesirable nuclear interference reactions) and irradiated during 3 h in the USGS TRIGA reactor, in Denver, Colorado (USA) or in the Oregon State University TRIGA reactor, in Corvallis, Oregon (USA). The mean J-values computed from standard grains within the small pits and determined as the average and standard deviation of J-values of the small wells for each irradiation disc are given along with the raw data. Mass discrimination for each sample was monitored using an automated air pipette and calculated relative to an air ratio of 298.56 ± 0.31(Lee et al. 2006). Correction factors for interfering isotopes were $(^{39}Ar/^{37}Ar)$ $Ca = 6.95 \times 10^{-4}$ ($\pm 1.3\%$), $(^{36}Ar/^{37}Ar)$ $Ca = 2.65 \times 10^{-4}$ ($\pm 0.84\%$) and $(^{40}Ar/^{39}Ar)$ $K = 7.30 \times 10^{-4}$ ($\pm 12.4\%$) (Renne et al. 2013) for the OSU reactor. The $^{40}Ar/^{39}Ar$ analyses were performed at the Western Australian Argon Isotope Facility at Curtin University on two different instruments (either a MAP 215-50 or an ARGUS VI), for which details are provided below. The raw data were processed using the ArArCALC software (Koppers 2002), and ages were calculated using decay constants recommended by Renne et al. (2011). All parameters and relative abundance values have been corrected for blank, mass discrimination and radioactive decay.

Our criteria for the determination of plateaus or concordant age populations (for single crystals analyses) are as follows: plateaus must include at least 70% of ^{39}Ar, and be distributed over a minimum of 3 consecutive steps that agreeing at 95% confidence levels and indicate a probability of fit (P value) of at least 0.05. Concordant single-crystal age population need to include three concordant ages and a P value of at least 0.05. Plateau ages

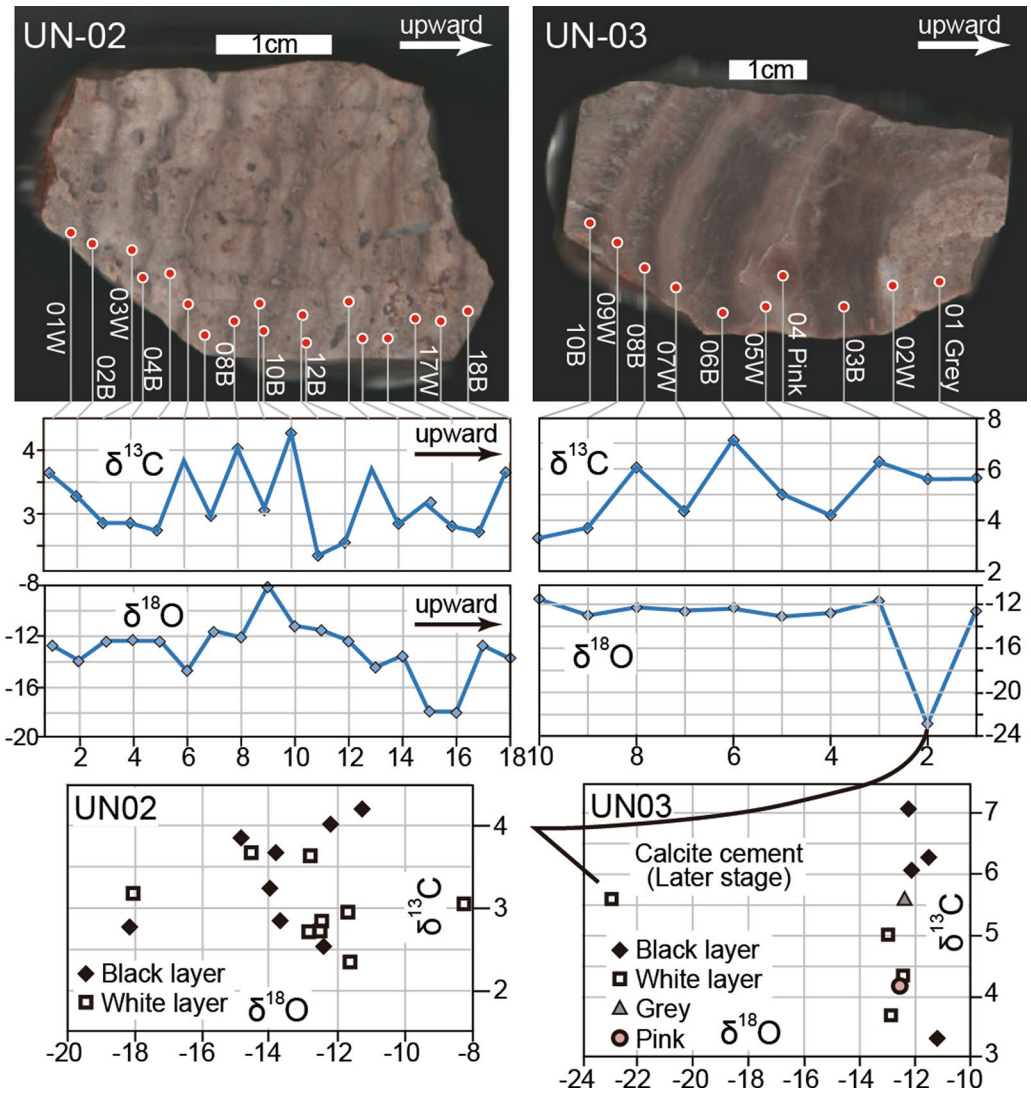

Fig. 4 Laminated structures and oxygen-carbon isotopes of two carbonate samples from Jiuziyan Formation

(Fig. 5) are given at the 2σ level and are calculated using the mean of all plateau steps, weighted by the inverse variances of their individual analytical uncertainties. Inverse isochrons include the maximum number of steps with a probability of fit ≥ 0.05. S-factors showing the spread along the inverse isochron (Jourdan et al. 2007), and $^{40}Ar/^{36}Ar$ intercept values are provided. Uncertainties include analytical and J-value errors; those that incorporate all sources of uncertainty are indicated by square brackets (e.g., [±3.0 ka]). Finally, all ages calculated in this study are all given at the 2σ level.

Pyroclastic flow (#140902-04)—this sample yielded a robust age of 35.74 ± 0.08 Ma ($n = 13/15$; $P = 0.57$) for the sanidine crystals and several age populations of 37.16 ± 0.25 Ma ($n = 7/15$; $P = 0.57$), 36.05 ± 0.40 Ma ($n = 3/15$; $P = 0.72$) and 25.3 ± 1.5 Ma ($n = 4/15$; $P = 0.91$) for the biotite crystals. We note that the sanidine age is in agreement with the biotite age population that returned an intermediate age, and since sanidine in general less easily affected by alteration and 39Ar recoil loss problems, we therefore believe that sanidine provides the best age estimates (35.74 ± 0.08 Ma) for the eruption of this volcanic tuff (Fig. 5A).

Trachyte intrusion (140902-5)—the sanidine population from this sample yielded a plateau age of 35.65 ± 0.09 Ma ($P = 0.14$) and an inverse isochron age of 35.75 ± 0.10 Ma ($P = 0.73$) with a 40Ar/36Ar intercept ratio of 290 ± 5 and a spreading factor of 25% anchored on the radiogenic axis (not shown).

Lamprophyre (#140903-5)—The muscovite population from this sample failed to give any plateau age and rather showed a diffusion profile converging toward an age of ~ 65 Ma.

Lamprophyre (#141021-01)—The biotite population from this sample did not yield any plateau age and showed a wavy spectra with individual step ages mostly distributed between 38 and 35 Ma (Fig. 5B).

3.2 Palynological study

One hundred and three samples were taken from the Cenozoic rocks for palynological identification. Standard preparation techniques were applied, including diluted hydrochloric acid digestion, hydrofluoric acid digestion, concentrated hydrochloric acid and enumerated using an OLYMPUS optical microscope at 400 × magnification. Seventy-six samples counted comprised in excess of 100 pollen grains, which were used to rebuild the vegetation in the region. A total of 73 pollen and spore types were enumerated, 53 to genus level. The pollen assemblages of different formations are described below (Fig. 6).

Yunlong Formation: The high proportion of conifer pollen like Pinus or xerophytic steppe elements dominated by *Artemisia* characterizes the Yunlong Formation, with deciduous broad-leaved tree like *Alnus* occurring in less amount. Others, like *Quercus*, Ulmaceae, and *Corylus/Carpinus* usually stay at low percentages. Pollen assemblage reflects the appearance of a pinewood or a sparse steppe environment, indicating relatively arid conditions.

Baoxiangsi Formation: The pollen assemblage consists mainly of *Pinus* and the deciduous broadleaved trees of *Alnus* with slightly more herbs of Poaceae than Yunlong Formation. In some intervals, assemblage is dominated by deciduous broadleaved trees of Ulmaceae with the xerophytic steppe elements of *Ephedra*. All together these represent a sparse forest environment, indicating a temperate environment.

In the eolian sand dune deposits of upper Baoxiangsi Formation, the high proportion of evergreen broadleaved tree like *Quercus* characterizes this zone, suggesting the development of subtropical forest and warm climate.

Jinsichang/Shuanghe Formation: The high proportion of deciduous broad-leaved trees of Ulmaceae characterizes this zone, together with conifer pollen like *Pinus*, *Picae*, and evergreen broad-leaved trees of *Quercus* occurred occasionally. The herb elements like Poaceae, Ranunculaceae and *Cyperus* have increased. Then, the dominating Polypodiaceae ferns appeared in this formation. The assemblage indicates distinctive of warm and humid/wet conditions, often rain forests.

3.3 Hematite /goethite ratios

Hematite and goethite are common in soil, being the weathering products of iron-bearing silicate, and are sensitive to climatic conditions. Arid, warm climates favor the formation of hematite, while cooler, humid climates result in the formation of more goethite. The hematite/goethite ratio increases as the annual temperature increases and soil moisture decreases.

Hematite and goethite concentrations were measured in the Key Laboratory of Surficial Geochemistry, Ministry of Education of China (at Nanjing University), by using PerkinElmer Lamda 900. Thirty-one samples from different stratigraphic positions were measured for hematite and goethite contents. In general, Yunlong and Baoxiangsi Formations have higher contents of hematite and lower content of goethite. More distinguishably, the hematite /goethite ratios of Yunlong and Baoxiangsi Formations are much higher than that of Jinsichang and Shuanghe Formations (Fig. 7B).

4 Discussions

4.1 Aridity during the early paleogene

Relatively arid climatic conditions in the SE Tibetan Plateau are inferred from the sedimentary facies of the Yunlong and Baoxiangsi Formations (Fig. 2B). Facies analysis indicates that the Yunlong Formation was deposited in a fluvial-lacustrine setting under a relatively arid regime, although one still requiring some precipitation. High contents of hematite and high degrees of redness of the sediments indicate strong oxidation (Fig. 7B). Pollen analysis reveals a sparse flora assemblage, with *Pinus*, *Alnus* and *Artemisia* indicating temperate conditions (Figs. 6 and 7C). Deposition of the Baoxiangsi Formation marks a new phase of basin development, with widespread fanglomerate and proximal sandstone representing initiation of uplift of the surrounding basement rocks as the pull-apart basin opened (Fig. 2B). Climatic conditions of lower Baoxiangsi Formation were generally similar to that of the Yunlong Formation, with redness, suggestive of hematite in the soil, indicative of oxidation, likely linked to at least seasonal aridity (Schwertmann 1971). *Pinus*, *Alnus* and Ulmaceae pollen indicate temperate conditions (Mathews et al. 2013). Aridity culminated during the deposition of upper Baoxiangsi Formation when eolian sand dunes were being developed, which indicates a desert environment (Fig. 3). Previous studies have revealed that similar desert and steep environments existed over a much broader region across China (Sun and Wang 2005; Zhang et al. 2012). This situation is interpreted to represent a climatic zone dominated by sub-tropical high pressure system.

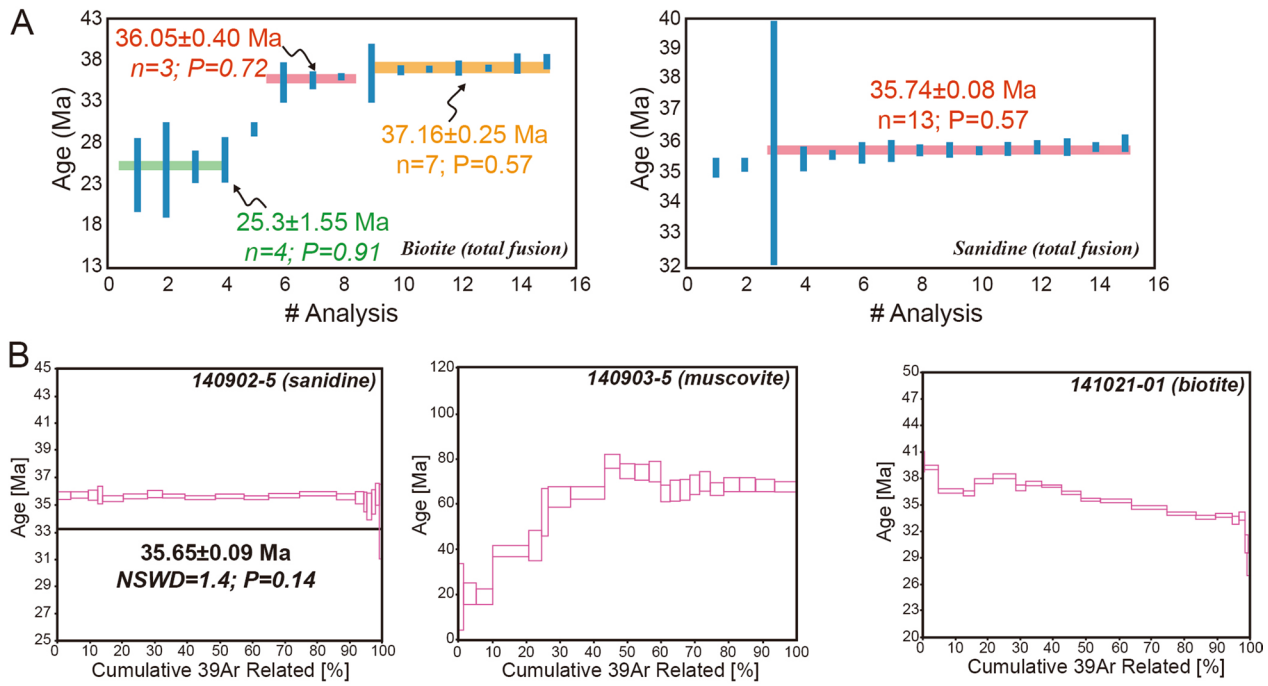

Fig. 5 **A** Total fusion analyses for biotite and sanidine crystals from sample #140902-04; **B** Sanidine, biotite and muscovite step-heating $^{40}Ar/^{39}Ar$ age spectra of samples #140902-05, #140903-5 and #141021-01

The Yunlong and Baoxiangsi Formations have previously been assigned Paleocene and Eocene ages, respectively, based on stratigraphic correlation, while the Shuanghe ages from Gourbet et al. (2017) only constrained this to be older than ~ 36 Ma. Radiometric dating of intrusions within the Baoxiangsi Formation presented here now provides much more precise age constraints for sedimentation and confirms that the upper Baoxiangsi Formation, including the eolian dune unit, was deposited during the mid to late Eocene, prior to 36 Ma.

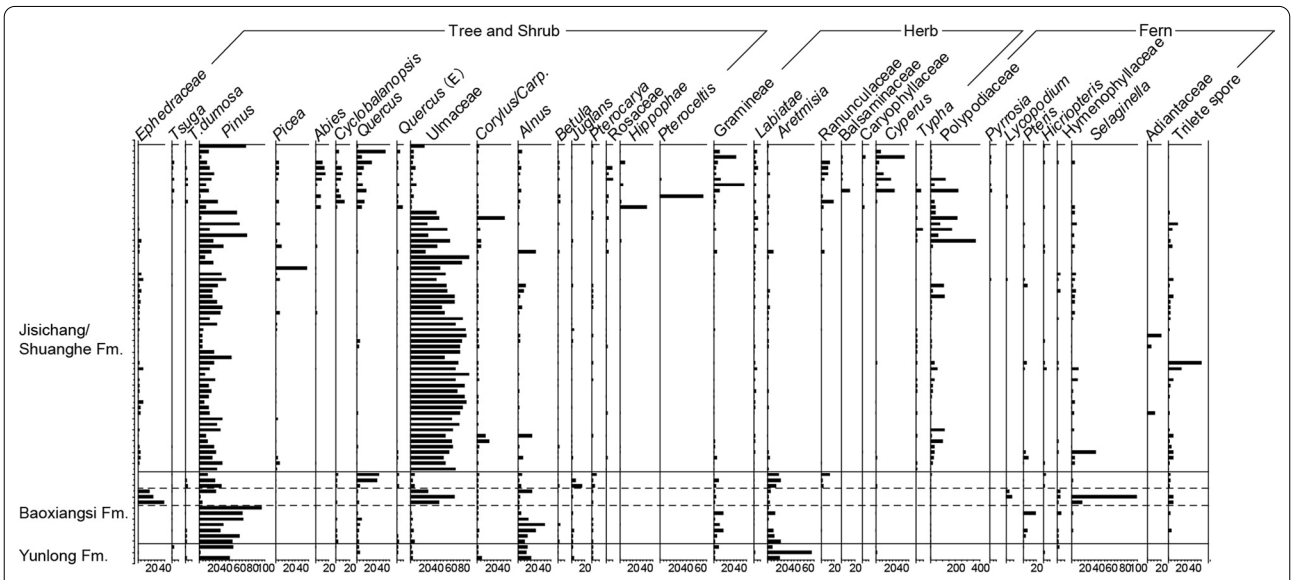

Fig. 6 Palynology study of Cenozoic sediments from Jianchuan Basin

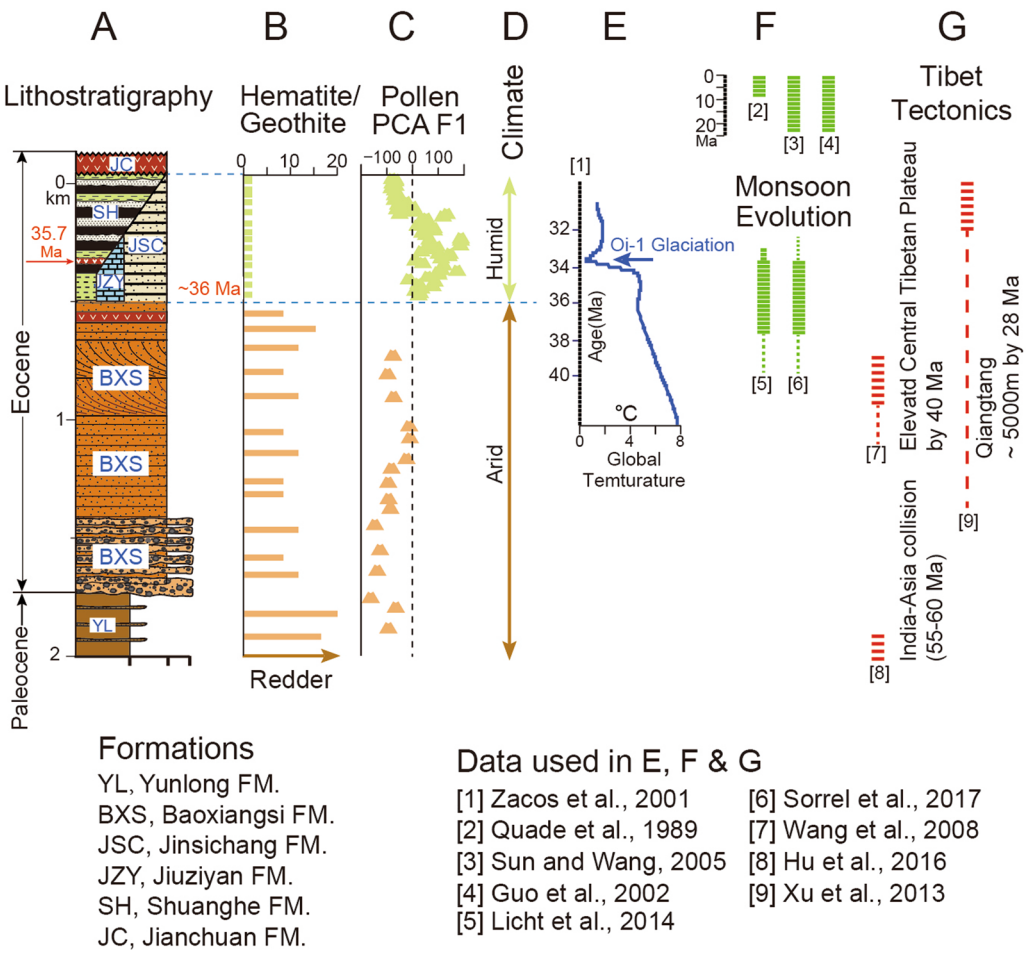

Fig. 7 Integrated Lithostratigraphy and data from Jianchuan Basin. **A** Lithostratigraphy of Jianchuan Basin; **B** Hematite/Geothite ratio; **C** The first principal component of pollen; **D** Interpretation of climatic conditions based on sedimentary facies and climatic proxies; **E** Global temperature curve modified from Zachos et al. (2001); **F** Evolution of Asian monsoon proposed by different authors; **G** Major tectonic-geomorphic events of Tibetan Plateau related to India-Asia collision. Note that the *Y* axis (age) in **F** is not proportional to depth in **A**

4.2 Onset of monsoon climate at ~ 36 Ma

Relatively humid climatic conditions are required to explain the facies of the Shuanghe, Jinsichang and Jiuziyan Formations (Fig. 2B). The Shuanghe coal beds, as discussed above, are typical of swamp and fluvial-lacustrine environments. Not only does the sedimentary facies indicate the existence of flowing, permanent water, but the pollen assemblage reveals a diverse ecosystem indicative of wet subtropical conditions (Fig. 6). Facies analysis of the Jinsichang Formation indicates that it was deposited within a large fluvial system, most likely dominated by braided rivers. The evidence indicates significant moisture supply to the region to sustain a lacustrine, swamp and significant fluvial system, which contrasts with the arid environments that characterized the Yunlong and Baoxiangsi Formations. Onset of monsoon climate would have greatly altered the ecosystem, promoting biodiversity in the region (Su et al. 2019).

4.3 Climatic transition at ~ 36 Ma: orography-versus global cooling-driven

In this study, we confirm not only the existence of humid conditions in the Late Eocene in the Jianchuan Basin, but critically also show for the first time a major climatic transition around 36 Ma (Fig. 7). The evidence for swampy and fluvial conditions is consistent with earlier research in the area (Tapponnieret al. 2001) and with indications of a wet monsoonal climate in Myanmar, as well as in NE Tibet at that time (Wan et al. 2007). Although Sorrel et al. (2017) suggested moderately drier conditions for the carbonates of the Jiuziyan Formation this interpretation is not consistent with this sediment being equivalent in time to the

Jinsichang and Shuanghe Formation. In any case, it is our identification of windblown desert dune sands that accumulated to a great thickness that provides concrete evidence for long-lived arid conditions in the mid to late Eocene, followed by a relatively rapid transition into a wetter monsoonal environment. Furthermore, the fact that these desert (arid) conditions extended over much of China indicates that this was significant climatic phenomena, and not just a local feature (Sun and Wang 2005). We note that this transition from dry to wet occurs at 36 Ma and therefore does not correlate with any significant change in the global climate. We noticed that Fang et al. (2021) proposed that this change could have occurred at ~ 41 Ma. The possible reason for the age discrepancy could have been caused by the complexity of the sedimentary sequences. More importantly and more precisely, as we have observed, the sedimentary sequences have been, in many places, misplaced due to faulting caused mostly by volcanism. It is an on-going mission to refine the chronology of the sequence. Our age control is based on dating of the volcanic rock (lamprophyre) that has been intruded into the sequence and the volcano-clastic rock that is interbedded in the sequence. In any of the cases, the transition contrasts with the proposed drying of the climate at 34 Ma, across the Eocene–Oligocene boundary, which correlates with a time of global cooling (Fig. 7) (Dupont-Nivet et al. 2007). Our reconstruction of a significant wettening of the climate does not correlate with a corresponding global temperature event (Zachos et al. 2001). Instead, it may well be attributed to the orographic effects of Himalaya and Tibetan Plateau. Uplift of parts the Tibetan Plateau at this time (Wang et al. 2008; Xu et al. 2013) is anticipated to have affected atmospheric circulation patterns and resulted in intensification of the East Asian monsoon, while deflecting the influence of the Westerly Jet (Fig. 1). It has been increasingly recognized that the Eo-Oligocene was a time of topographic uplift of the plateau and it is possible that this had progressed to a critical level of altitude and extent where a rapid transition from dry and wet conditions occurred (Wang et al. 2008; Xu et al. 2013; Prell and Kutzbach 1992; Liu et al. 2017). The change from arid into humid conditions represents a cessation of dominance by the sub-tropical high pressure system in controlling the climate of Southeast Asia, even if the summer monsoon had not yet reached maximum intensity (Additional file 1).

5 Conclusions

Cenozoic sedimentary rocks from the southeast flank of Tibetan Plateau record a drastic climatic change from general aridity to monsoonal conditions around 36 Ma. Paleocene aridity belonged to a much broader arid zone across East Asia, which was formed under the influence of northern sub-tropical high pressure system when Tibetan Plateau was not high and extensive enough to obstruct the general circulation. Uplift of Tibetan Plateau might have reached a threshold elevation during late Eocene, which deflected the Westerly Jet and altered the general circulation system, causing the inception or significant intensification of monsoonal rains to penetrate into this downwind locality through thermal and dynamic forcing.

Abbreviations

XB: Xining Basin; MB: Myanmar Basin; FM: Formation; S: Superimposition surface; gf: Grainfall and grainflow strata; wr: Wind ripple strata; R: Reactivation surfaces; I: Interdune migration surfaces; SEM: Scanning electron microscope; FCs: Fish Canyon sanidine; YL: Yunlong formation; BXS: Baoxiangsi formation; JSC: Jinsichang formation; JZY: Jiuziyan formation; SH: Shuanghe formation; JC: Jianchuan formation.

Supplementary Information

The online version contains supplementary material available at https://doi.org/10.1186/s40645-022-00470-x.

Additional file 1. Supplementary materials.

Acknowledgements

We thank the two reviewers for constructive comments. We thank Bin Wang for his comments regarding the interpretation of climatic transition. PDC thanks the Charles T. McCord Jr chair in petroleum geology at LSU for support.

Authors' contributions

HZ designed research; HZ, QY, SC, PDC, MH, AK, RT and FJ performed research; HZ, QY, SC and PCD wrote the paper. All authors read and approved the final manuscript.

Funding

This work was jointly supported by the National Natural Science Foundation of China (41991323, U1902208 and 41888101), the Strategic Priority Research Program of Chinese Academy of Sciences (XDB26020301), the Second Tibetan Plateau Scientific Expedition and Research (STEP) (2019QZKK0704) and Yunnan Leading Talent Project (for H. Z.).

Data availability

All the data presented in this paper are available via the Mendeley database (http://dx.doi.org/10.17632/6mvhzzjdzv.1).

Declarations

Competing interests

The authors declare that they have no known competing financial interests or personal relationships that could have appeared to influence the work reported in this paper.

Author details
[1]Yunnan Key Laboratory of Earth System Science, Yunnan University, Kunming 650500, China. [2]School of Earth and Environmental Sciences, The University of Queensland, Brisbane, QLD 4072, Australia. [3]School of Earth Sciences, China University of Geosciences, Beijing 100083, China. [4]Department of Geology and Geophysics, Louisiana State University, Baton Rouge, LA 70803, USA. [5]School of Geography Science, Nanjing Normal University, Nanjing 210023, China. [6]Department of Earth and Planetary Science, University of Tokyo, Tokyo 113-0033, Japan. [7]Institute for Geo-Cosmology, Chiba Institute of Technology, 2-17-1 Tsudanuma, Narashino, Chiba 275-0016, Japan. [8]Western Australian Argon Isotope Facility, Department of Applied Geology and JdL Centre, Curtin University, Perth, WA 6845, Australia.

Received: 25 August 2021 Accepted: 27 January 2022
Published online: 16 February 2022

References

Boos WR, Kuang Z (2010) Dominant control of the South Asian monsoon by orographic insulation versus plateau heating. Nature 463(7278):218–222. https://doi.org/10.1038/nature08707

Brookfield ME, Silvestro S (2010) Eolian systems. In: Darlymple RW, James NP (eds) Facies models. Geological Association of Canada, Newfoundland and Labrador

Carmichael MJ, Lunt DJ, Huber M, Heinemann M, Kiehl J et al (2016) A model–model and data–model comparison for the early Eocene hydrological cycle. Clim past 12:455–481

Clift PD, Shimizu N, Layne GD, Blusztajn JS, Gaedicke C, Schlüter HU et al (2001) Development of the Indus Fan and its significance for the erosional history of the western Himalaya and Karakoram. Geol Soc Am Bull 113(8):1039–1051. https://doi.org/10.1130/0016-7606(2001)113%3c1039:DOTIFA%3e2.0.CO;2

Clift PD, Hodges KV, Heslop D, Hannigan R, Van Long H, Calves G (2008) Correlation of Himalayan exhumation rates and Asian monsoon intensity. Nature Geosci 1:875–880. https://doi.org/10.1038/ngeo351

Curray JR, Emmel FJ, Moore DG (2002) The Bengal Fan: morphology, geometry, stratigraphy, history and processes. Mar Petrol Geol 19(10):1191–1223. https://doi.org/10.1016/S0264-8172(03)00035-7

DeCelles PG, Kapp P, Gehrels GE, Ding L (2014) Paleocene-Eocene foreland basin evolution in the Himalaya of southern Tibet and Nepal: implications for the age of initial India-Asia collision. Tectonics 33(5):824–849. https://doi.org/10.1002/2014tc003522

Dupont-Nivet G, Krijgsman W, Langereis CG, Abels HA, Dai S, Fang X (2007) Tibetan plateau aridification linked to global cooling at the Eocene–Oligocene transition. Nature 445(7128):635–638. https://doi.org/10.1038/nature05516

Fang X, Yan M, Zhang W, Nie J, Han W, Wu F, Song C, Zhang T, Zan J, Yang Y (2021) Paleogeography control of Indian monsoon intensification and expansion at 41 Ma. Science Bulletin 66:2320–2328. https://doi.org/10.1016/j.scib.2021.07.023

Garzanti E (2018) Petrographic classification of sand and sandstone. Earth-Sci Rev 192:545–563. https://doi.org/10.1016/j.earscirev.2018.12.014

Gat J R (1980) The isotopes of hydrogen and oxygen in precipitation. In: Fritz P, Fontes JC (eds) Handbook of Environmental Geochemistry, vol 1: The terrestrial environment. ScienceDirect, pp 21–47. https://doi.org/10.1016/B978-0-444-41780-0.50007-9

Guo ZT, Ruddiman WF, Hao QZ, Wu HB, Qiao YS, Zhu RX, Peng SZ, Wei JJ, Yuan Y, Liu TS (2002) Onset of Asian desertification by 22 Myr ago inferred from loess deposits in China. Nature 416(6877):159–163. https://doi.org/10.1038/416159a

Gourbet L, Leloup PH, Paquette JL, Sorrel P, Maheo G, Wang G, Xu YD, Cao K, Anroine PO, Eymard I, Liu W, Lu H, Replumaz A, Chevalier ML, Zhang K, Wu J, Shen TY (2017) Reappraisal of the Jianchuan Cenozoic basin stratigraphy and its implications on the SE Tibetan plateau evolution. Tectonophysics 700:162–179. https://doi.org/10.1016/j.tecto.2017.02.007

Gupta AK, Yuvaraja A, Prakasam M, Clemens SC, Velu A (2015) Evolution of the South Asian monsoon wind system since the late Middle Miocene. Palaeogeogr Palaeocl 438:160–167. https://doi.org/10.1016/J.PALAEO.2015.08.006

Hu X, Garzanti E, Wang J, Huang W, An W, Webb A (2016) The timing of India-Asia collision onset—facts, theories, controversies. Earth-Sci Rev 160:264–299. https://doi.org/10.1016/J.EARSCIREV.2016.07.014

Huber M, Goldner A (2012) Eocene monsoons. J Asian Earth Sci 44:3–23

Jourdan F, Féraud G, Bertrand H, Watkeys M, Renne PR (2007) Distinct brief major events in the Karoo large igneous province clarified by new $^{40}Ar/^{39}Ar$ ages on the Lesotho basalts. Lithos 98(1):195–209. https://doi.org/10.1016/j.lithos.2007.03.002

Koppers AAP (2002) ArArCALC-software for $^{40}Ar/^{39}Ar$ age calculations. Comput Geosci 28(5):605–619. https://doi.org/10.1016/S0098-3004(01)00095-4

Kroon D, Steens T, Troelstra SR (1991) Onset of monsoonal related upwelling in the western Arabian sea as revealed by planktonic foraminifers. Proc Odp Sci Results 117:257–263. https://doi.org/10.2973/odp.proc.sr.117.126.1991

Lee JY, Marti K, Severinghaus JP, Kawamura K, Yoo HS, Lee JB, Kim JS (2006) A redetermination of the isotopic abundances of atmospheric Ar. Geochim Cosmochim Acta 70(17):4507–4512. https://doi.org/10.1016/J.GCA.2006.06.1563

Li D, Huang X, Wang A, Yu S (1988) Discovery and significance of Paleocene marine facies limestone in northwest Yunnan. Sci Bull 9:763–768

Licht A, Cappelle M, Abels HA, Ladant JB, Trabucho-Alexandre J, France-Lanord C, Donnadieu Y, Vandenberghe J, Rigaudier T, Lécuyer C, Terry JD, Adriaens R, Boura A, Guo Z, Soe AN, Quade J, Dupont-Nivet G, Jaeger JJ (2014) Asian monsoons in a late Eocene greenhouse world. Nature 513(7519):501–506. https://doi.org/10.1038/nature13704

Liu X, Dong B, Yin ZY, Smith RS, Guo Q (2017) Continental drift and plateau uplift control origination and evolution of Asian and Australian monsoons. Sci Rep 7(1):40344. https://doi.org/10.1038/srep40344

Liu Z, Sun H, Baoying L, Xiangling L, Wenbing Y, Cheng Z (2010) Wet-dry seasonal variations of hydrochemistry and carbonate precipitation rates in a travertine-depositing canal at Baishuitai, Yunnan, SW China: implications for the formation of biannual laminae in travertine and for climatic reconstruction. Chem Geol 273(3–4):258–266. https://doi.org/10.1016/j.chemgeo.2010.02.027

Loope DB, Rowe CM, Joeckel RM (2001) Annual monsoon rains recorded by Jurassic dunes. Nature 412(6842):64–66. https://doi.org/10.1038/35083554

Mathews RP, Tripathi SM, Banerjee S, Dutta S (2013) Palynology, palaeoecology and palaeodepositional environment of Eocene lignites and associated sediments from Matanomadh mine, Kutch Basin, western India. J Geol Soc India 82(3):236–248. https://doi.org/10.1007/s12594-013-0146-z

Miall AD (1977) A review of the braided-river depositional environment. Earth-Sci Rev 13(1):1–62. https://doi.org/10.1016/0012-8252(77)90055-1

Molnar P, Boos WR, Battisti DS (2010) Orographic controls on climate and paleoclimate of Asia: thermal and mechanical roles for the Tibetan Plateau. Annu Rev Earth Planet Sci 38(1):77–102. https://doi.org/10.1146/annurev-earth-040809-152456

Morley C (2002) A tectonic model for the Tertiary evolution of strike-slip faults and rift basins in SE Asia. Tectonophysics 347(4):189–215. https://doi.org/10.1016/S0040-1951(02)00061-6

Mountney NP (2012) A stratigraphic model to account for complexity in aeolian dune and interdune successions. Sedimentology 59(3):964–989. https://doi.org/10.1111/j.1365-3091.2011.01287.x

Najman Y (2006) The detrital record of orogenesis: a review of approaches and techniques used in the Himalayan sedimentary basins. Earth-Sci Rev 74:1–72. https://doi.org/10.1016/J.EARSCIREV.2005.04.004

Najman Y, Appel E, Boudagher-Fadel M, Bown P, Carter A, Garzanti E, Godin L, Han J, Liebke U, Oliver G, Parrish R, Vezzoli G (2010) Timing of India-Asia collision: Geological, biostratigraphic, and palaeomagnetic constraints. J Geophys Res. https://doi.org/10.1029/2010JB007673

Prell WL, Kutzbach JE (1992) Sensitivity of the Indian monsoon to forcing parameters and implications for its evolution. Nature 360(6405):647–652. https://doi.org/10.1038/360647a0

Prell WL, Murray DW, Clemens SC, Anderson DM (1992) Evolution and variability of the Indian ocean summer monsoon: evidence from the western Arabian sea drilling program. In: Duncan RA, Rea DK, Kidd RB, von Rad U, Weissel JK (eds) Synthesis of Results from Scientific Drilling in the Indian Ocean. vol 70, pp 447–469. https://doi.org/10.1029/GM070p0447

Quade J, Cerling TE, Bowman JR (1989) Development of Asian monsoon revealed by marked ecological shift during the latest Miocene in northern Pakistan. Nature 342(6246):163–166. https://doi.org/10.1038/342163A0

Rea DK (1994) The paleoclimatic record provided by eolian deposition in the deep sea: The geologic history of wind. Rev Geop 32(2):159–195. https://doi.org/10.1029/93RG03257

Renne PR, Balco G, Ludwig KR, Mundil R, Min K (2011) Response to the comment by W.H. Schwarz et al. on "Joint determination of 40K decay constants and $^{40}Ar^*/^{40}K$ for the Fish Canyon sanidine standard, and improved accuracy for $^{40}Ar/^{39}Ar$ geochronology" by P.R. Renne et al. (2010). Geochim Cosmochim Acta 75(17):5097–5100. https://doi.org/10.1016/j.gca.2011.06.021

Renne PR, Deino AL, Hilgen FJ, Kuiper KF, Mark DF, Mitchell III WS, Morgan LE, Mundil R, Smit J (2013) Time scales of critical events around the Cretaceous-Paleogene boundary. Science 339(6120):684–687

Rozanski K, Araguás-Araguás L, Gonfiantini R (1993) Isotope patterns in modern global precipitation. In: Swart PK, Lohmann KL, McKenzie J, Savin S (eds) climate change in continental isotope records, vol 78. American Geophysical Union, Washington, pp 1–37. https://doi.org/10.1029/GM078p0001

Sakuma A, Kano A, Kakizaki Y, Tada R, Zheng H (2021) Upper Eocene travertine-lacustrine carbonate in the Jianchuan basin, southeastern Tibetan Plateau: reappraisal of its origin and implication for the monsoon climate. Island Arc 30(1):e12416. https://doi.org/10.1111/iar.12416

Schwertmann U (1971) Transformation of hematite to goethite in soils. Nature 232(5313):624–625. https://doi.org/10.1038/232624a0

Smith DG (1987) Meandering river point bar lithofacies models: modern and ancient examples compared. SEPM Spec Publ 39:83–91. https://doi.org/10.1038/232624a0

Sorrel P, Eymard IPM, Leloup PH, Maheo G, Olivier N, Sterb M, Lu H (2017) Wet tropical climate in SE Tibet during the Late Eocene. Sci Rep 7(1):7809–7809. https://doi.org/10.1038/s41598-017-07766-9

Spicer RA, Yang J, Herman AB, Kodrul T, Maslova N, Spicer TEV, Aleksandrova G, Jin J (2016) Asian Eocene monsoons as revealed by leaf architectural signatures. Earth Planet Sci Lett 449:61–68. https://doi.org/10.1016/j.epsl.2016.05.036

Su T, Spicer RA, Li SH, Xu H, Huang J, Sherlock S, Huang YJ, Li SF, Wang L, Jia LB et al (2019) Uplift, climate and biotic changes at the Eocene-Oligocene transition in south-eastern Tibet. Natl Sci Rev 6(3):495–504. https://doi.org/10.1093/nsr/nwy062

Sun X, Wang P (2005) How old is the Asian monsoon system? -Palaeobotanical records from China. Palaeogeogr Palaeocl 222(3):181–222. https://doi.org/10.1016/J.PALAEO.2005.03.005

Tada R, Zheng H, Clift PD (2016) Evolution and variability of the Asian monsoon and its potential linkage with uplift of the Himalaya and Tibetan Plateau. Progr Earth Planet Sci 3(1):4. https://doi.org/10.1186/S40645-016-0080-Y

Talbot MR (1990) A review of the palaeohydrological interpretation of carbon and oxygen isotopic ratios in primary lacustrine carbonates. Chem Geol Isotope Geosci Sect 80(4):261–279. https://doi.org/10.1016/0168-9622(90)90009-2

Tapponnier P, Zhiqin X, Roger F, Meyer B, Arnaud N, Wittlinger G, Jingsui Y (2001) Oblique stepwise rise and growth of the Tibet Plateau. Science 294(5547):1671–1677. https://doi.org/10.1126/SCIENCE.105978

Wan S, Li A, Clift PD, Stuut JBW (2007) Development of the East Asian monsoon: mineralogical and sedimentologic records in the northern South China Sea since 20 Ma. Palaeogeogr Palaeocl 254(3):561–582. https://doi.org/10.1016/j.palaeo.2007.07.009

Wang B (2010) The Asian monsoon. Springer, Berlin. https://doi.org/10.1007/3-540-37722-0

Wang C, Zhao X, Liu Z, Lippert PC, Graham SA, Coe RS, Yi H, Zhu L, Liu S, Li Y (2008) Constraints on the early uplift history of the Tibetan Plateau. P Natl Acad Sci USA 105(13):4987–4992. https://doi.org/10.1073/PNAS.0703595105

Webster PJ, Magaña VO, Palmer TN, Shukla J, Tomas RA, Yanai M, Yasunari T (1998) Monsoons: processes, predictability, and the prospects for prediction. J Geophys Res 103:14451–14510. https://doi.org/10.1029/97JC02719

Wu FY, Ji WQ, Wang JG, Liu CZ, Chung SL, Clift PD (2014) Zircon U-Pb and Hf isotopic constraints on the onset time of India-Asia collision. Am J Sci 314(2):548–579. https://doi.org/10.2475/02.2014.04

Xu Q, Ding L, Zhang L, Cai F, Lai Q, Yang D, Liu-Zeng J (2013) Paleogene high elevations in the Qiangtang Terrane, central Tibetan Plateau. Earth Planet Sc Lett 362:31–42. https://doi.org/10.1016/j.epsl.2012.11.058

Yang TN, Liang MJ, Fan JW, Shi PL, Zhang HR, Hou ZH (2014) Paleogene sedimentation, volcanism, and deformation in eastern Tibet: evidence from structures, geochemistry, and zircon U-Pb dating in the Jianchuan basin. SW China Gondwana Res 26(2):521–535. https://doi.org/10.1016/j.gr.2013.07.014

Yunnan Bureau of Geology and Mineral Resources (1990) 1:200000 regional map series and accompanying reports, 728. Geological Publishing House, Beijing **(in Chinese)**

Zachos J, Pagani M, Sloan L, Thomas E, Billups K (2001) Trends, rhythms, and aberrations in global climate 65 Ma to present. Science 292(5517):686–693. https://doi.org/10.1126/SCIENCE.1059412

Zhang Z, Flatøy F, Wang H, Bethke I, Bentsen M, Guo Z (2012) Early Eocene Asian climate dominated by desert and steppe with limited monsoons. J Asian Earth Sci 44:24–35. https://doi.org/10.1016/j.jseaes.2011.05.013

Zheng H, Clift PD, He M, Bian Z, Liu G, Liu X, Jourdan F (2020) Formation of the first bend in the late Eocene gave birth to the modern Yangtze River. Geology, China. https://doi.org/10.1130/G48149.1

Publisher's Note